

## On the Gamma-Ray Emission of the Andromeda Galaxy M31

YI XING,<sup>1</sup> ZHONGXIANG WANG,<sup>2,1</sup> DONG ZHENG,<sup>2</sup> AND JIE LI<sup>3,4</sup>

<sup>1</sup>Key Laboratory for Research in Galaxies and Cosmology, Shanghai Astronomical Observatory, Chinese Academy of Sciences, 80 Nandan Road, Shanghai 200030, China; yixing@shao.ac.cn; wangzx20@ynu.edu.cn

<sup>2</sup>Department of Astronomy, School of Physics and Astronomy, Yunnan University, Kunming 650091, China

<sup>3</sup>Laboratory for Research in Galaxies and Cosmology, Department of Astronomy, University of Science and Technology of China, Hefei 230036, China

<sup>4</sup>School of Astronomy and Space Science, University of Science and Technology of China, Hefei 230026, China

### ABSTRACT

Using the  $\gamma$ -ray data obtained with the Large Area Telescope (LAT) onboard the *Fermi Gamma-ray Space Telescope (Fermi)* for  $\sim 14$  years, we examine the high energy emission emanating from the center of the Andromeda Galaxy M31. Different from previously reported results, which show a seemingly extended source, we instead find two individual point sources, one consistent with being at the center and one  $0^\circ.4$  south-east of the center. The emission of the former is well described using a Log-Parabola model, similar to those of previous studies, and that of the latter can be fitted with a power law. We discuss the possible origins for the two sources. M31's central source, now consistent with being a point source, necessitates a revisit of its previously discussed originations with this new property taken into consideration, in particular those cosmic rays or dark matter scenarios involving extended source distributions. The SE source appears to have a projected distance of  $\sim 6$  kpc from M31's center, and the investigation is required as to whether it is a source locally associated with M31, or is instead a background extra-galactic one.

*Keywords:* Gamma-ray sources (633); Andromeda Galaxy (39)

### 1. INTRODUCTION

The Andromeda Galaxy M31, located approximately 780 kpc away from our Milky Way (Conn et al. 2012), is one of a dozen galaxies that have been detected at  $\gamma$ -rays (Xi et al. 2020; Abdollahi et al. 2022). Utilizing the 2-yr data taken with the Large Area Telescope (LAT) onboard the *Fermi Gamma-ray Space Telescope (Fermi)*, the *Fermi*-LAT Collaboration (Abdo et al. 2010) first reported the detection of M31 at a  $5\sigma$  confidence level. Following this initial report, different analyses of the LAT data have been performed for studies of the  $\gamma$ -ray emission of M31 (Li et al. 2016; Pshirkov et al. 2016; Ackermann et al. 2017; Karwin et al. 2019; Zimmer et al. 2022). It appears that the primary  $\gamma$ -ray emission of M31 coincides with its center, and efforts have been made to identify a possible extended structure in the emission, whose presence in M31 is expected and would reveal the existence and distribution of cosmic rays or supposedly massive dark matter. Due to the hadronic and/or leptonic processes of the former (e.g., McDaniel et al. 2019; Do et al. 2021) or the decay or annihilation of the latter (e.g.,

Beck & Colafrancesco 2017; McDaniel et al. 2018), the observed  $\gamma$ -ray emission may be explained.

Among the reported analyses and results, a representative analysis was provided by the *Fermi*-LAT Collaboration in Ackermann et al. (2017). Using  $> 7$ -yr LAT data, they tested a list of different point and extended source models in their analysis. They found that the  $\gamma$ -ray emission of M31 was consistent with it being at the center and described with a  $0^\circ.38$ -radius uniform-brightness disk (at a  $4\sigma$  significance level).

Now with  $\sim 14$  years of  $\gamma$ -ray data collected with LAT, we conducted analysis for studying the  $\gamma$ -ray emission of M31, and found that rather than one extended source, the emission stems actually from two sources, one at the center and one south-east to the center. In this paper, we report the analysis and results of this study. Below Section 2 describes our analysis of the LAT data and provides the results, and in Section 3, we discuss the results and their implications for our understanding of M31's  $\gamma$ -ray emission.

### 2. FERMI LAT DATA AND ANALYSIS

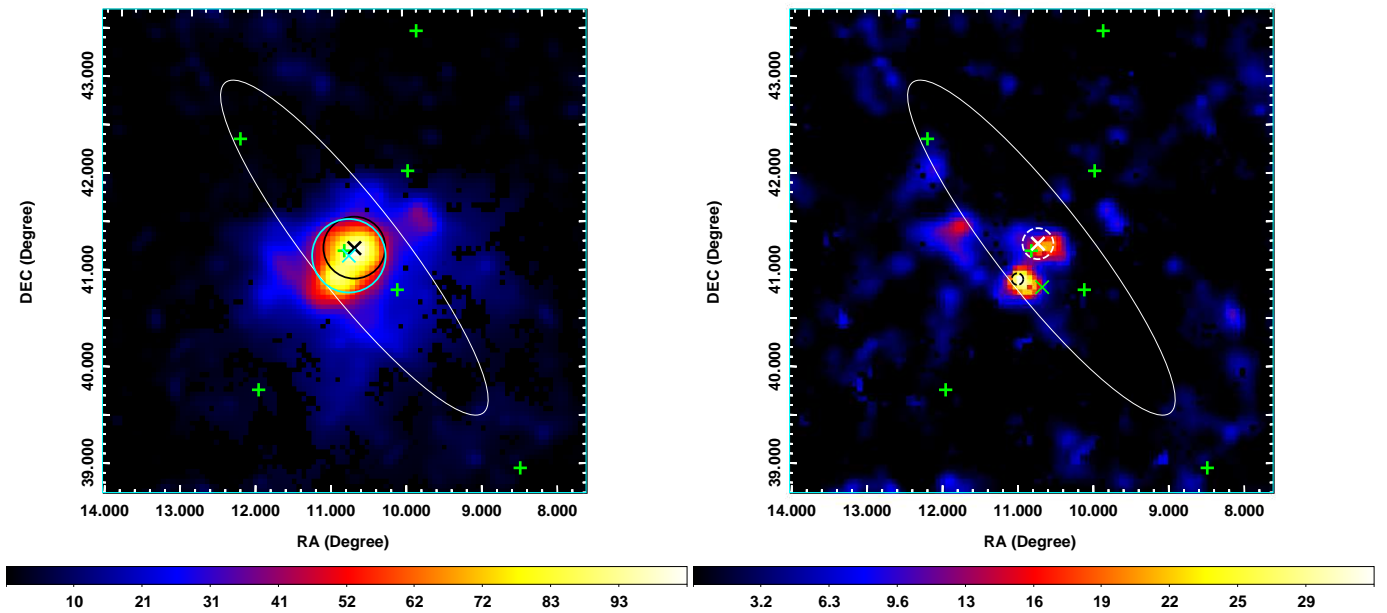


**Figure 1.** TS maps for the region of M31 in the energy ranges of 0.1–500 GeV (*left* panel) and 2–500 GeV (*right* panel). The image scale of each TS map is  $0.05 \text{ degree pixel}^{-1}$ , for which a color bar is drawn to indicate the TS value range. Also in each TS map, a white ellipse is plotted to show the M31 disk/halo boundary defined in Racine (1991) and green pluses to show the 4FGL-DR3 catalog sources, which include M31 (the center one in the ellipse). *Left:* a cyan cross and circle mark the best-fit uniform-brightness disk model given in Ackermann et al. (2017), and a black cross and circle the best-fit disk model we determined (note the black cross is fixed at the central position of M31 given in SIMBAD database; cf., Section 2.3). *Right:* a white cross and dashed circle mark the position and  $2\sigma$  error circle respectively we determined for the M31 central emission, and a black dashed circle marks the  $2\sigma$  error circle for the SE source. In addition, the position of M32 is marked by a green cross.

### 2.1. LAT Data and Baseline Source Model

We selected 0.1–500 GeV LAT events from the updated *Fermi* Pass 8 database in the time period from 2008-08-04 15:43:39 (UTC) to 2022-09-26 23:16:35 (UTC). The region of interest (ROI) was set to be centered at M31’s catalog position with a size of  $20^\circ \times 20^\circ$ , and the *CLEAN* event class was used in the analysis. As recommended by the LAT team<sup>1</sup>, we included events with zenith angles less than 90 deg so as to prevent the Earth’s limb contamination, and we also excluded events with ‘bad’ quality flags.

In the *Fermi* LAT 12-yr source catalog (4FGL-DR3; Abdollahi et al. 2022), the  $\gamma$ -ray counterpart to M31 is listed as a point source (PS) modeled with a Log-Parabola (LP) spectral form,  $dN/dE = N_0(E/E_b)^{-(\alpha+\beta \log(E/E_b))}$ . We considered this PS model as a baseline one (named 1PS) for M31 and made our source model by including all sources listed in 4FGL-DR3 within 20 deg of M31. The spectral forms and parameters of the sources are provided in the catalog.

<sup>1</sup> <http://fermi.gsfc.nasa.gov/ssc/data/analysis/scitools/>

Unless stated otherwise, for our analysis, spectral parameters were always set free for the sources within 5 deg of M31, while the rest were fixed at their catalog values. The spectral model *gll\_iem\_v07.fit* was used for the Galactic diffuse emission, and the spectral file *iso\_P8R3\_CLEAN\_V3\_v1.txt* was used for the extragalactic diffuse emission, with their normalizations both set free.

### 2.2. One Point Source Analysis

We performed the standard binned likelihood analysis to the LAT data in the 0.1–500 GeV band using the 1PS source model, where the scale parameter  $E_b$  in the LP model for M31 was fixed to the catalog value of 913.08 MeV. For M31’s  $\gamma$ -ray emission, we obtained  $\alpha = 2.2 \pm 0.2$ ,  $\beta = 0.36 \pm 0.16$ , and 0.1–500 GeV photon flux  $F_{\text{ph}} = 2.7 \pm 1.2 \times 10^{-9} \text{ photon cm}^{-2} \text{ s}^{-1}$ , which are consistent with those give in the catalog. The Test Statistic (TS) value obtained for the source was 108, wherein the likelihood value  $L_{1\text{PS}} (= 177565.02)$  was used for model comparisons below in Section 2.3. We tested the effects of setting  $E_b$  free, and found the results to be nearly the same, only with larger uncertain-

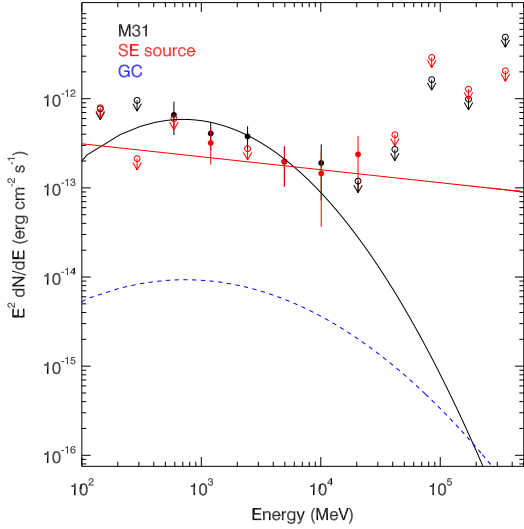


**Figure 2.**  $\gamma$ -ray spectra of the central M31 and SE sources (black squares and red dots respectively), along which the flux upper limits are shown as the open symbols. The best-fit models for the two sources, the LP for the M31 central one and PL for the SE one, are shown as the black curve and red line respectively. For comparison, the model spectrum of our Galactic center source (4FGL J1745.6–2859) given in Abdollahi et al. (2022) is scaled by the distance ratio  $(8 \text{ kpc}/780 \text{ kpc})^2$  and shown as a blue dashed curve.

ties. This indicates that the fitting was not sensitive to this parameter given the relatively low TS value of the source. As such, we fixed  $E_b$  at the catalog value for the following analysis.

To carefully examine the analysis results, we calculated a 0.1–500 GeV TS map for a  $5^\circ \times 5^\circ$  region centered at M31, in which all the catalog sources except M31 were removed. The TS map, shown in the left panel of Figure 1, seemingly suggests that the  $\gamma$ -ray emission at the central position of M31 is extended, though slightly elongating along the south-east (SE) direction. We mark the best-fit, uniform-brightness disk (radius  $0^\circ 38$ ) reported in Ackermann et al. (2017) with a cyan circle in the figure, and as shown, the disk does enclose the emission. However, when we checked the TS maps at higher energy ranges, we found that the  $\gamma$ -ray emission in fact is resolved to be two individual sources. In the right panel of Figure 1, we show a similar TS map but with an energy range in 2–500 GeV. As can be seen, one source is at the center of M31, and the other one is SE to the center. We ran *gtfindsrc* in *Fermitools* to the 2–500 GeV data to determine the position of this SE source, and obtained R.A.= $11^\circ 01$ , Decl.= $+40^\circ 95$ , (equinox J2000.0). The  $1\sigma$  nominal uncertainty for the position was  $\simeq 0^\circ 03$ .

### 2.3. Verification Analysis for Two Point Sources

Since the discovery of two sources can critically change our understanding of M31’s  $\gamma$ -ray emission, we conducted various analyses to verify our results. First, we re-performed the maximum likelihood analysis with 2 PSs included in the source model (named 2PS) this time. The source at the center of M31 was still set to have a LP spectral form, while the SE source at the position obtained above was modeled with a simple power law (PL). We obtained  $\alpha = 2.1 \pm 0.3$ ,  $\beta = 0.27 \pm 0.14$ , and  $F_{\text{ph}} = 2.4 \pm 1.3 \times 10^{-9} \text{ photon cm}^{-2} \text{ s}^{-1}$  for the center one, with  $\text{TS} \simeq 79$ , and for the SE one, we obtained PL index  $\Gamma = 2.1 \pm 0.2$  and  $F_{\text{ph}} = 1.7 \pm 1.1 \times 10^{-9} \text{ photon cm}^{-2} \text{ s}^{-1}$  with  $\text{TS} \simeq 35$ . These results are summarized in Table 1. We compared the likelihood value  $L_{2\text{PS}}$ , from the 2PS model, to  $L_{1\text{PS}}$  using the formula  $\sqrt{2(\log L_{2\text{PS}} - \log L_{1\text{PS}})}$ , and found the fit improved at a  $6.0\sigma$  significance level.

We then proceeded to compare the 2PS model with the best-fit uniform-brightness disk model reported in Ackermann et al. (2017). We included the disk (centered at R.A.= $10^\circ 76$ , Decl.= $41^\circ 19$ ; note that this position has SE offsets from the central position of M31) in the source model, whose spectral form was a LP, and obtained a TS value of 152 from the likelihood analysis (the parameter values are given in Table 1). In comparing the likelihood values from this disk model and the 2PS model, the latter was found to be better at a  $3.7\sigma$  confidence level.

Finally, we also tested a uniform-brightness disk with the center fixed at that of M31 given in the SIMBAD<sup>2</sup> database. The radius of the disk was searched from  $0^\circ 00$  (i.e., a PS) to  $0^\circ 70$  with a step of  $0^\circ 02$ . Comparison of the resulting likelihood values indicated that the best fit was obtained when the radius was  $0^\circ 32$ , while the TS value was 138. When comparing this best fit to the 2PS model, the likelihood values indicated that the latter was better at a  $5.0\sigma$  significance level.

Given the clear indications of two sources in the 2–500 GeV TS map, verified further with the additional analyses, we concluded that there are two  $\gamma$ -ray sources in the direction of M31. We then proceeded to check whether the central source at M31 would be extended or not. Once again, we included the SE one as a PS in the source model and set a uniform-brightness disk for the central one, with the radius varied in the same manner as the above, and then performed the likelihood analysis. Going over the results, no significant extendedness was found for the central source. Therefore

<sup>2</sup> <http://simbad.u-strasbg.fr/simbad/>

this  $\gamma$ -ray source at M31's center is a PS based on the *Fermi* LAT data. Furthermore by running `gtfindsrc` to the 2–500 GeV data, we also obtained its position: R.A.=10 $^{\circ}$ 73, Decl.=+41 $^{\circ}$ 32 (equinox J2000.0), with a  $2\sigma$  error radius of 0 $^{\circ}$ 16 (shown in the right panel of Figure 1). This position is consistent with that of the center of M31.

#### 2.4. Spectral Analysis

We extracted the  $\gamma$ -ray spectra of the two sources by performing the maximum likelihood analysis of the LAT data in 12 evenly divided energy bands in logarithm from 0.1–500 GeV. In the extraction, the spectral normalizations of sources within 5 deg of M31's catalog position were set as free parameters, while all other source parameters were fixed at values obtained from the above likelihood analysis. A PL spectral form was set for the two sources, with  $\Gamma$  fixed to 2. For the obtained spectral data points, we kept those with  $\text{TS} \geq 4$  and derived 95% flux upper limits for the rest. Figure 2 shows the spectra, and Table 2 provides the flux (or upper limit) values and their respective TS values.

The respective best-fit LP and PL spectral models for M31's central and SE sources, obtained from the above 2PS-model analysis, are also plotted in Figure 2. As shown, the best-fit models adequately describe the  $\gamma$ -ray spectra. We also tested other often-used spectral models for each of the two sources, for example a PL and a PL with an exponentially cutoff (PLEC) for the M31's central one. We did not find that other models were better. The LP and PLEC models provided equally good fits to the emission of M31's central source, and then the both were better than a PL at a  $2.7\sigma$  significance level. All three models provided a nearly equally well fit for the emission of the SE source, which was likely due to the low TS value ( $\simeq 35$ ) of the source.

#### 2.5. Variability Analysis

As a check, we searched for long-term variability of the two sources in 0.1–500 GeV by calculating Variability Index  $\text{TS}_{var}$  (Nolan et al. 2012). We extracted light curves of 87 time bins, with each bin consisting of 60-day data. Following the procedure introduced in Nolan et al. (2012), if the flux of a source is constant,  $\text{TS}_{var}$  would be distributed as  $\chi^2$  with 86 degrees of freedom; variable sources would be identified when  $\text{TS}_{var}$  is larger than 119.4 (at a 99% confidence level). The computed  $\text{TS}_{var}$  for the M31 central and SE sources were 73.1 and 76.4 respectively, indicating that the two sources did not show significant long-term flux variations.

### 3. DISCUSSION

After analyzing the  $\sim 14$ -yr *Fermi* LAT data for the M31 region, we obtained the results different to those of previous reports. There are two sources contained in the  $\gamma$ -ray emission of M31, one at the center and one with offsets of 0 $^{\circ}$ 33 in R.A. and  $-0^{\circ}$ 32 in Decl. from the center. As the central one is brighter, its emission is still described with a LP model consistent with the previous ones (including that given in the 4FGL-DR3; Abdollahi et al. 2022). The emission of the SE one is described with a PL model, and one feature can be noted is that its emission contains high energy photons in  $\sim 15$ –30 GeV (cf., Figure 2 and Table 2). The findings thus drastically change the perception of M31's  $\gamma$ -ray emission.

As the central emission is consistent with being a PS, limiting its origin to M31's central region, the source of the emission should be located within  $\sim 2.2$  kpc of the center (at a source distance of 780 kpc) by considering the  $2\sigma$  error radius of 0 $^{\circ}$ 16. The origins involving some degree of extended distributions, such as cosmic rays (McDaniel et al. 2019; Do et al. 2021) or dark matter (e.g., Beck & Colafrancesco 2017; McDaniel et al. 2018) in M31 should be revisited (also see Ackermann et al. 2017 and references therein). Another possible origin discussed is the old population of unresolved objects in the center, such as millisecond pulsars (MSPs; e.g., Ackermann et al. 2017; Eckner et al. 2018), since one competing scenario for the excess  $\gamma$ -ray emission of our own Galactic center is that the emission arises from MSPs (Brandt & Kocsis 2015). We note that given the 0.1–500 GeV flux of  $1.9 \times 10^{-12}$  ergs $^{-1}$  cm $^{-2}$  obtained from the 2PS model for the central source, its  $\gamma$ -ray luminosity is  $\simeq 1.4 \times 10^{38}$  ergs $^{-1}$ . This luminosity is much larger than those of known  $\gamma$ -ray sources in our Galaxy. For example, the luminosity is  $\sim 50$  times that of our Galactic center emission (cf., Figure 2), which is the most luminous one at  $\gamma$ -rays in our Galaxy (Cafardo et al. 2021; Abdollahi et al. 2022). Thus in order to explain the central emission of M31 with those of a population of MSPs, the number of MSPs would be required to be at least 15000 (Xing et al., in preparation, where the estimation method is fully described in Wu et al. 2022). Whether the central region of M31 can host such a large number of MSPs is uncertain (Fragione et al. 2019).

Though the SE source is significantly away from the center of M31, it still appears to be within the M31's galactic region (cf., Figure 1). Given that 6659 sources have been detected with LAT in the all sky (Abdollahi et al. 2022), the average source density is  $\sim 0.16$  deg $^{-2}$ . Considering a circle of 0 $^{\circ}$ 4 radius (the distance between the center of M31 and the SE source),

the chance of finding two or more sources in such a circular region by coincidence is  $\sim 0.4\%$ . Thus there is a high chance that the SE source is associated with M31. Its 0.1–500 GeV flux is  $\simeq 1.5 \times 10^{-12} \text{ erg s}^{-1} \text{ cm}^{-2}$ , implying the luminosity would be  $\sim 1.0 \times 10^{38} \text{ erg s}^{-1}$  at M31’s distance. This luminosity is still much larger than that of any Galactic source, which renders it difficult to identify its possible source types via simple property comparisons between the SE source and the luminous Galactic sources. We searched for sources within the SE source’s  $2\sigma$  error circle in other bands. At the optical bands, there are two globular clusters (GCs) given in the SIMBAD database; however, associating the  $\gamma$ -ray emission with the GCs is difficult as a large number of MSPs would be required to be contained in them (e.g., Wu et al. 2022). At the X-ray band, Stiele et al. (2011) reported the results from the deep *XMM-Newton* survey of M31. In their results, there were 12 X-ray sources within the error circle; among them, three were classified as foreground star candidates, one as a galaxy candidate, and eight had unknown classes. The last eight sources were generally faint, having X-ray fluxes of  $2\text{--}7 \times 10^{-15} \text{ erg s}^{-1} \text{ cm}^{-2}$ . It is not clear whether one of them, located away from M31’s center with projected distances of  $\sim 6 \text{ kpc}$ , could be the counterpart to the  $\gamma$ -ray source.

Alternatively, if we consider the low probability that the SE source is a background extra-galactic one, we first note that while the SE source’s position is close, it does not coincide with that of the galaxy M32 (cf., right panel of Figure 1). Since in the  $\gamma$ -ray sky, dom-

inant extra-galactic sources are Active Galactic Nuclei (AGN; Abdollahi et al. 2022) with demonstrably significant radio emission (i.e., having radio jets; e.g., de Menezes et al. 2020), we checked for the radio sources within the error circle and found four listed in either the SIMBAD database (Bystedt et al. 1984; Braun 1990) or the Very Large Array Sky Survey Epoch 1 catalog (Gordon et al. 2020). Among them, one is the galaxy candidate previously mentioned, and the other three do not have obvious X-ray or optical counterparts. As given in Stiele et al. (2011), the X-ray position of this galaxy candidate is R.A.=10°985375, Decl.=40°9815833, (equinox J2000.0), with a  $3\sigma$  nominal uncertainty of  $3''74$ , but looking into the determined radio or optical positions for this galaxy, we find that the X-ray error circle does not enclose the positions. The properties of this source remain to be further investigated. In conclusion, while the SE source has the properties of exhibiting a hard spectrum and constant  $\gamma$ -ray emission over the past 14 years, its nature is uncertain.

This research has made use of the SIMBAD database, operated at CDS, Strasbourg, France.

This work is support by the Basic Research Program of Yunnan Province (No. 202201AS070005), the National Natural Science Foundation of China (12273033), and the Original Innovation Program of the Chinese Academy of Sciences (E085021002).

## REFERENCES

- Abdo, A. A., Ackermann, M., Ajello, M., et al. 2010, *A&A*, 523, L2, doi: [10.1051/0004-6361/201015759](https://doi.org/10.1051/0004-6361/201015759)
- Abdollahi, S., Acero, F., Baldini, L., et al. 2022, *ApJS*, 260, 53, doi: [10.3847/1538-4365/ac6751](https://doi.org/10.3847/1538-4365/ac6751)
- Ackermann, M., Ajello, M., Albert, A., et al. 2017, *ApJ*, 836, 208, doi: [10.3847/1538-4357/aa5c3d](https://doi.org/10.3847/1538-4357/aa5c3d)
- Beck, G., & Colafrancesco, S. 2017, *JCAP*, 2017, 007, doi: [10.1088/1475-7516/2017/10/007](https://doi.org/10.1088/1475-7516/2017/10/007)
- Brandt, T. D., & Kocsis, B. 2015, *ApJ*, 812, 15, doi: [10.1088/0004-637X/812/1/15](https://doi.org/10.1088/0004-637X/812/1/15)
- Braun, R. 1990, *ApJS*, 72, 761, doi: [10.1086/191432](https://doi.org/10.1086/191432)
- Bystedt, J. E. V., Brinks, E., de Bruyn, A. G., et al. 1984, *A&AS*, 56, 245
- Cafardo, F., Nemmen, R., & Fermi LAT Collaboration. 2021, *ApJ*, 918, 30, doi: [10.3847/1538-4357/ac0efe](https://doi.org/10.3847/1538-4357/ac0efe)
- Conn, A. R., Ibata, R. A., Lewis, G. F., et al. 2012, *ApJ*, 758, 11, doi: [10.1088/0004-637X/758/1/11](https://doi.org/10.1088/0004-637X/758/1/11)
- de Menezes, R., Nemmen, R., Finke, J. D., Almeida, I., & Rani, B. 2020, *MNRAS*, 492, 4120, doi: [10.1093/mnras/staa083](https://doi.org/10.1093/mnras/staa083)
- Do, A., Duong, M., McDaniel, A., et al. 2021, *PhRvD*, 104, 123016, doi: [10.1103/PhysRevD.104.123016](https://doi.org/10.1103/PhysRevD.104.123016)
- Eckner, C., Hou, X., Serpico, P. D., et al. 2018, *ApJ*, 862, 79, doi: [10.3847/1538-4357/aac029](https://doi.org/10.3847/1538-4357/aac029)
- Fragione, G., Antonini, F., & Gnedin, O. Y. 2019, *ApJL*, 871, L8, doi: [10.3847/2041-8213/aafc62](https://doi.org/10.3847/2041-8213/aafc62)
- Gordon, Y. A., Boyce, M. M., O’Dea, C. P., et al. 2020, *Research Notes of the American Astronomical Society*, 4, 175, doi: [10.3847/2515-5172/abbe23](https://doi.org/10.3847/2515-5172/abbe23)
- Karwin, C. M., Murgia, S., Campbell, S., & Moskalenko, I. V. 2019, *ApJ*, 880, 95, doi: [10.3847/1538-4357/ab2880](https://doi.org/10.3847/1538-4357/ab2880)
- Li, Z., Huang, X., Yuan, Q., & Xu, Y. 2016, *JCAP*, 2016, 028, doi: [10.1088/1475-7516/2016/12/028](https://doi.org/10.1088/1475-7516/2016/12/028)
- McDaniel, A., Jeltama, T., & Profumo, S. 2018, *PhRvD*, 97, 103021, doi: [10.1103/PhysRevD.97.103021](https://doi.org/10.1103/PhysRevD.97.103021)

- . 2019, *PhRvD*, 100, 023014,  
doi: [10.1103/PhysRevD.100.023014](https://doi.org/10.1103/PhysRevD.100.023014)
- Nolan, P. L., Abdo, A. A., Ackermann, M., et al. 2012,  
*ApJS*, 199, 31, doi: [10.1088/0067-0049/199/2/31](https://doi.org/10.1088/0067-0049/199/2/31)
- Pshirkov, M. S., Vasiliev, V. V., & Postnov, K. A. 2016,  
*MNRAS*, 459, L76, doi: [10.1093/mnrasl/slw045](https://doi.org/10.1093/mnrasl/slw045)
- Racine, R. 1991, *AJ*, 101, 865, doi: [10.1086/115731](https://doi.org/10.1086/115731)
- Stiele, H., Pietsch, W., Haberl, F., et al. 2011, *A&A*, 534,  
A55, doi: [10.1051/0004-6361/201015270](https://doi.org/10.1051/0004-6361/201015270)
- Wu, W., Wang, Z., Xing, Y., & Zhang, P. 2022, *ApJ*, 927,  
117, doi: [10.3847/1538-4357/ac4f48](https://doi.org/10.3847/1538-4357/ac4f48)
- Xi, S.-Q., Zhang, H.-M., Liu, R.-Y., & Wang, X.-Y. 2020,  
*ApJ*, 901, 158, doi: [10.3847/1538-4357/aba043](https://doi.org/10.3847/1538-4357/aba043)
- Zimmer, F., Macias, O., Ando, S., Crocker, R. M., &  
Horiuchi, S. 2022, *MNRAS*, 516, 4469,  
doi: [10.1093/mnras/stac2464](https://doi.org/10.1093/mnras/stac2464)

**Table 1.** Likelihood analysis results

Source Model	$2\log(L/L_{1PS})$	Parameters			
		$\alpha$	$\beta$	$F^*/10^{-9}$	TS
1PS	0	$2.2\pm 0.2$	$0.36\pm 0.16$	$2.7\pm 1.2$	108
2PS M31	36	$2.1\pm 0.3$	$0.27\pm 0.14$	$2.4\pm 1.3$	79
SE		$2.1^*\pm 0.2$		$1.7\pm 1.1$	35
Disk <sub>0.38</sub> <sup>†</sup>	22	$2.1\pm 0.1$	$0.13\pm 0.09$	$4.8\pm 1.4$	152
Disk <sub>M31</sub> <sup>‡</sup>	11	$2.2\pm 0.1$	$0.21\pm 0.10$	$4.2\pm 1.3$	138

<sup>†</sup>Disk model reported in [Ackermann et al. \(2017\)](#). <sup>‡</sup>Disk model we tested with the center fixed at the central position of M31. \*0.1–500 GeV photon flux in units of  $\text{photon cm}^{-2} \text{s}^{-1}$ . \*Value of photon index  $\Gamma$  in the power-law model.

**Table 2.** Flux Measurements for the central source of M31 and the SE source

GeV	$G_{M31}$	TS	$G_{SE}$	TS
0.14 (0.1–0.2)	0.77	0	0.79	0
0.29 (0.1–0.4)	0.96	1	0.21	0
0.59 (0.4–0.8)	$0.66\pm 0.27$	20	0.60	2
1.20 (0.8–1.7)	$0.41\pm 0.14$	15	$0.32\pm 0.13$	9
2.44 (1.7–3.5)	$0.38\pm 0.11$	19	0.28	2
4.96 (3.5–7.1)	$0.20\pm 0.09$	9	$0.20\pm 0.10$	8
10.08 (7.1–14.4)	$0.19\pm 0.12$	7	$0.15\pm 0.11$	4
20.50 (14.4–29.2)	0.12	0	$0.24\pm 0.15$	11
41.70 (29.2–59.5)	0.27	0	0.39	0
84.79 (59.5–120.9)	1.6	0	2.9	1
172.42 (120.9–245.9)	1.0	0	1.3	0
350.63 (245.9–500.0)	4.9	1	2.1	0

Notes:  $G$  is the energy flux ( $E^2 dN/dE$ ) in units of  $10^{-12} \text{ erg cm}^{-2} \text{ s}^{-1}$ . Fluxes without uncertainties are the 95% upper limits.